Inducible Site-Selective Bottom-Up Assembly of Virus-Derived Nanotube Arrays on RNA-Equipped Wafers

Anna Mueller,[†,⊥] Fabian J. Eber,[†,⊥] Carlos Azucena,[‡,⊥] Andre Petershans,[‡,⊥] Alexander M. Bittner,[§] Hartmut Gliemann,[‡,*] Holger Jeske,[†] and Christina Wege[†,*]

[†]Department of Molecular Biology and Virology of Plants, Institute of Biology, Universität Stuttgart, Pfaffenwaldring 57, 70569 Stuttgart, Germany, [‡]Institute of Functional Interfaces, Karlsruhe Institute of Technology (KIT), Hermann-von-Helmholtz-Platz 1, 76344 Eggenstein-Leopoldshafen, Germany, and [§]CIC nanoGUNE Consolider, Tolosa Hiribidea 76, 20018 Donostia, San Sebastian, and IKERBASQUE, Basque Foundation for Science, 48011 Bilbao, Spain. [⊥]These authors contributed equally to this work.

ABSTRACT Tobacco mosaic virus (TMV) is a tube-shaped, exceptionally stable plant virus, which is among the biomolecule complexes offering most promising perspectives for nanotechnology applications. Every viral nanotube self-assembles from a single RNA strand and numerous identical coat protein (CP) subunits. Here we demonstrate that biotechnologically engineered RNA species containing the TMV origin of assembly can be selectively attached to solid surfaces *via* one end and govern the bottom-up growth of surface-linked TMV-like nanotubes *in situ* on demand. SiO_2 wafers patterned by polymer blend lithography were modified in a chemically selective manner, which allowed positioning of *in vitro* produced RNA scaffolds into predefined patches on the 100−500 nm scale. The RNA operated as guiding strands for the self-assembly of spatially ordered nanotube 3D arrays on the micrometer scale. This novel approach may promote technically applicable production routes toward a controlled integration of multivalent biotemplates into miniaturized devices to functionalize poorly accessible components prior to use. Furthermore, the results mark a milestone in the experimental verification of viral nucleoprotein complex self-assembly mechanisms.

KEYWORDS: TMV-like particles · bottom-up assembly · nanotube array · biotemplate · Si wafer · polymer blend lithography

Central aims of current research efforts in the field of nanotechnology are the assembly of selectively addressable three-dimensional structures on the nanometer scale and their precise, spatially selective integration into microdevices.[1,2] Their directed arrangement and functionalization at predefined sites inside, however, still remains a challenge.[3,4] Tobacco mosaic virus[5] (TMV) and TMV derivatives are among the biomolecule complexes offering the most promising perspectives for applications as nanosized multivalent carrier templates for the presentation of functional molecules[6−10] and have proven substantial long-time stability in technical environments.[11,12] The tube-shaped, exceptionally robust plant virus has a natural length of 300 nm, a diameter of 18 nm, and an inner 4 nm wide channel. Its protein shell consists of ∼2100 identical CP subunits helically arranged on an RNA strand. The particle forms *via* self-assembly nucleated by the interaction of an RNA motif folding into characteristic secondary structures (origin of assembly, OAs) and assembly competent protein aggregates.[13] The entropy-driven process[14] has been analyzed extensively by *in vitro* studies, resulting in a widely accepted mechanistic model (as reviewed in detail[13]). Accordingly, 34 TMV CP subunits associate with a double-layered disk, which strongly interacts with the OAs. Upon a transition of the double-disk into a helical "lockwasher", the 5′ portion of the RNA is pulled "up" through the hole, allowing further CP disks to be concomitantly added to one end of the growing nanotube, intruding and coiling the RNA strand into the proteinaceous shell. Different from this mechanism of the RNA's 5′ end encapsidation, its 3′ end is thought to be packaged slowly by CP of lower oligomerization state and thus to remain accessible until the process is complete (compare to Figure 1). Our strategy is based on this assumption.

We have, for the first time, proven the hence expected capacity of TMV particles to grow autonomously on RNA immobilized *via* one end. The approach constitutes an attractive alternative route for the production of substrate-linked nanotubes, which might be combined with the manifold strategies already developed for their employment as carrier architectures presenting different functional molecules in technical contexts.[8,10,15−23] So far, a number of methods have allowed patterning of preassembled viral particles on surfaces.[8,24−32] The applicability of such arrays as templates for the production of battery electrodes has been described.[25,33] In some studies, TMV rods were immobilized following partial

* Address correspondence to hartmut.gliemann@kit.edu, christina.wege@bio.uni-stuttgart.de.

Received for review December 21, 2010 and accepted May 17, 2011.

Published online May 17, 2011
10.1021/nn103557s

© 2011 American Chemical Society

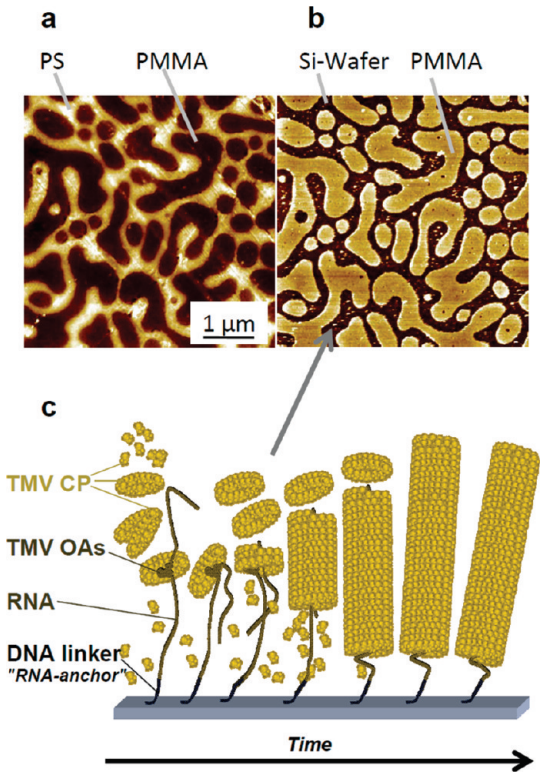

Figure 1. Experimental principles of inducible, RNA-guided bottom-up assembly of surface-linked TMV-derived nanotubes, spatially directed to surface patches predefined by polymer blend lithography. (a) AFM topography image after spin coating a SiO_2 substrate with a solution of the two immiscible polymers polystyrene (PS) and polymethylmethacrylate (PMMA) and demixing of the polymers. (b) Same area after selective PS removal by cyclohexane. Uncovered substrate areas are accessible and suitable for bottom-up self-assembly of virus-like nanotubes, as inferred from current models of TMV nucleoprotein assembly[13] (schematic drawing in panel c). Uncovered SiO_2 patches were functionalized and covalently equipped with DNA linker molecules, the ends of which were then ligated to RNA containing the TMV OAs. Finally, TMC CP was added under conditions initiating and sustaining their assembly with RNA.

disassembly, thus uncovering a portion of their RNA which was then hybridized to DNA bound to a solid support.[28,32,34]

Our work, in contrast, is a real bottom-up self-assembly approach for the site-selective RNA-guided fabrication of TMV-derived nanotube arrays on technically useful substrates. The procedure is based on the aforementioned assumption that the 3′ end of an OAs-containing RNA does not need any degree of freedom upon scaffolding the growth of TMV-like nucleoprotein tubes and might thus be immobilized without abolishing the process. Hence, appropriately engineered, noninfectious RNA constructs were bound to chemically modified SiO_2 substrates *via* immobilized DNA linkers, and purified TMV CP was added under conditions driving bottom-up self-assembly of virus-like nanotubes. Homogeneously functionalized wafers as well as specimens patterned on the sub-500 nm scale by

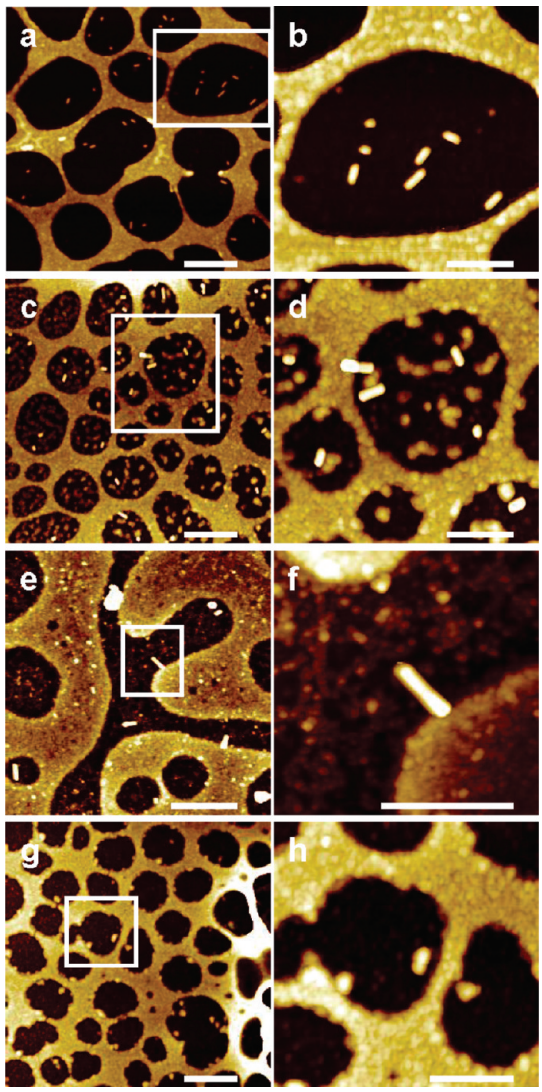

Figure 2. (a,c,e) AFM topography images of different SiO_2 substrates which were prepared identically. All substrates were structured by polymer blend lithography and utilized for bottom-up self-assembly of TMV-like nanotubes. The corresponding magnifications of the areas marked with a white frame are shown in panels b, d, and f, respectively. The substrate shown in panel g was prepared in the absence of DNA linkers, (h) zoom-in of panel g. Scale bars = 500 nm (a,c,e,g) or 250 nm (b,d,f,h).

polymer blend lithography were included in the study, as detailed in the following, and analyzed by atomic force microscopy (AFM) after CP multimerization reactions.

RESULTS AND DISCUSSION

Suitable surfaces were generated by coating Si wafers with aminopropyltriethoxysilane, the amino functions of which were reacted with glutardialdehyde.[35] In order to achieve spatially selective biotemplate growth, prestructured surfaces allowing site-specific binding of the DNA linkers were prepared. To this goal, Si wafers were patterned by polymer blend lithography[36–38] prior to the chemical functionalization.

The technique is suitable to create chemical surface textures of highly different dimensions and shapes. Parameters influencing the morphology of the resulting patterns have been discussed elaborately[39,40] and include the choice of solvents, polymer concentration, substrate coating speed, and humidity of the atmosphere. Polymer blend lithography can be used with almost any substrate sizes ranging from millimeters to meters and thus makes up a method of choice also for the high-throughput production of large-area array devices to be equipped with nanoscaled functions.

Si wafers were spin-coated by a blend of the two immiscible polymers polystyrene (PS) and polymethylmethacrylate (PMMA) dissolved in methyl−ethyl−ketone (MEK). Demixing of the polymers occurred upon fast evaporation of the solvent and resulted in patterns characteristic of the respective mixtures applied (Figure 1a). Cyclohexane treatment selectively removed PS, partially uncovering the Si wafer. Figures 1a,b represent the same area of a wafer exhibiting a characteristic circular and meander structure, before and after PS removal, respectively, leaving a PMMA mask 8−13 nm in height. The uncovered areas were aldehyde-functionalized. as described above.

Both homogeneous and patterned substrates were then set up for the initiation of RNA-guided viral nanotube self-assembly (process depicted in Figure 1c). ssDNA linker molecules ("RNA-anchor") with 3′-terminal amino modification were covalently bound to the aldehyde-functionalized areas of the wafers by condensation to Schiff bases (imines), the reaction conditions of which were optimized in our system (see Experimental Methods, and Supporting Information Figure S1). 5′-Phosphate residues of the DNA linkers permitted subsequent enzymatic ligation of assembly-triggering ssRNA strands *via* their 3′-terminal hydroxyl groups by T4 RNA ligase directly on the Si wafers (Figure 1c). The ssRNA utilized contained the TMV OAs sequence and was derived from *in vitro* transcription reactions with accordingly cloned and digested plasmid constructs (Experimental Methods[41]). Its size of 2884 nts was expected to direct the self-assembly of TMV-like nanotubes with a predicted maximum final length of 135 nm.[41]

Preparations of assembly competent TMV CP monomers[41] were then added to the RNA-equipped Si wafers under conditions favoring the growth of TMV particles in order to initiate and promote packaging of the immobilized RNA strands into nanotubes on the array surface (Figure 1c). The self-assembly of TMV-like nucleoprotein complexes generates free energy which intrudes and coils suitable RNA strands into the nascent nanotubes in solution. It was unknown, however, if in the surface-linked situation the respective forces were sufficient to overcome lateral unspecific physisorption of the RNA scaffold to the substrate − a well-known obstacle for many applications of nucleic acid

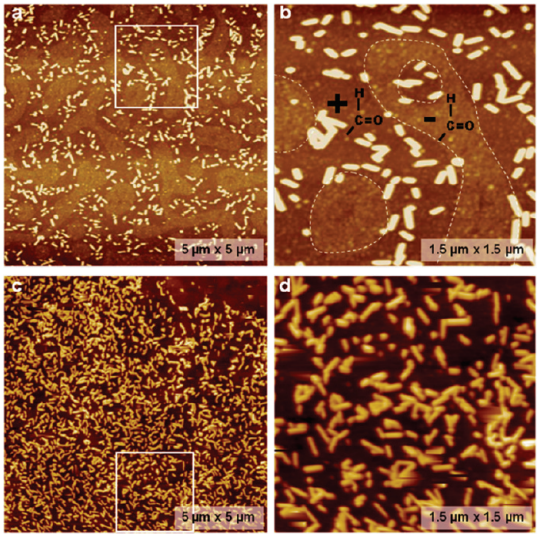

Figure 3. AFM topography image of TMV-like nanotubes on structured Si wafers. (a) PMMA mask was removed prior to nucleic acid linkage and TMV rod assembly induction, resulting in an increased density of site-selectively immobilized TMV-like nanorods on those areas which were functionalized with the aldehyde and equipped with DNA linkers plus RNA. (b) Zoom-in of the marked area in panel a, with dashed lines representing borders between initially aldehyde-terminated areas (+CHO; with DNA linker and RNA), and nonfunctionalized areas (−CHO), as indicated. (c) Substrate was prepared as in panel a; however, no RNA was immobilized on the DNA-functionalized areas, but preassembled VLPs were adsorbed, resulting in a nonspecific adhesion all over the substrate without spatial selectivity. (d) Zoom-in of the area marked with a white box in panel c. Height scale is 20 nm in all AFM images.

arrays.[42] AFM images of wafers subjected to the CP multimerization step revealed that, indeed, rod-like structures of homogeneous diameter had been assembled in the aldehyde-functionalized areas of the homogeneous (Supporting Information Figure S2) as well as of the prepatterned wafers (Figure 2a−f).

According to the AFM data, the rod-shaped nanoscopic elements had the expected width, after tip deconvolution, of *ca.* 20 nm.

Importantly, no rod-like structures were observed in control experiments, during which ssDNA linker molecules had been omitted (Figure 2g,h; Supporting Information Figure S2c) and in upstream steps prior to CP addition (data not shown), verifying that the novel structures represented TMV-CP-containing nanotubes grown bottom-up on an immobilized RNA scaffold. To ensure assembly competence of the virus-derived building blocks applied to the solid substrates, also non-immobilized RNA was incubated with coat protein in solution under conditions favoring nanotube growth in all experiments. The presence of tubular reaction products was verified by TEM (not shown, and see below in Figure 5). This demonstrates for the first time that a two-phase assembly of virus-like particles (VLP) from TMV-derived building blocks is mechanistically and energetically possible, with guiding

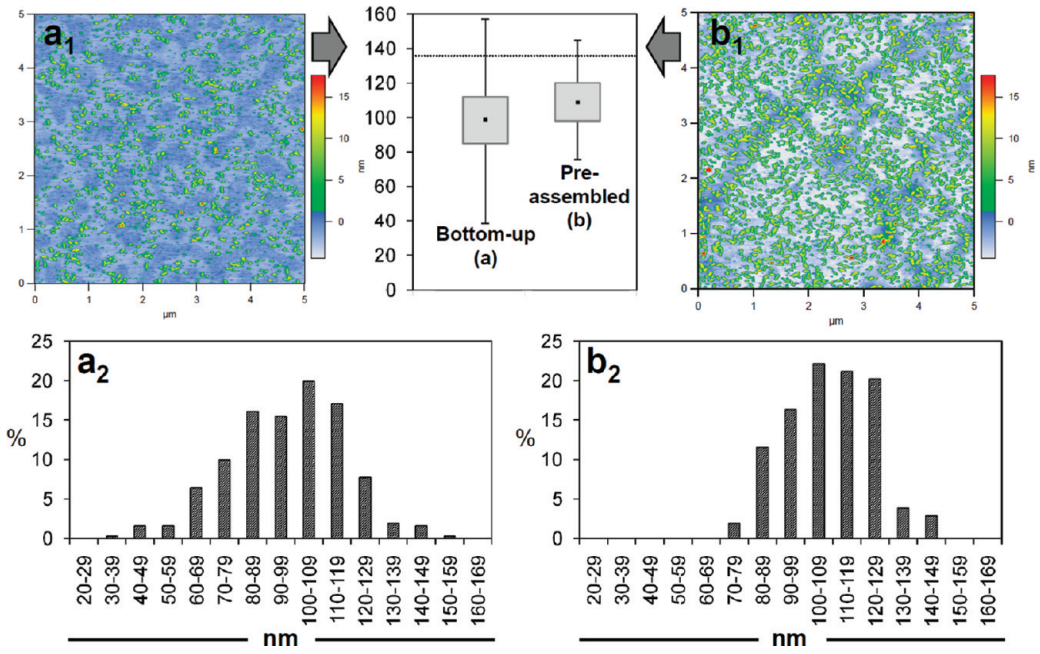

Figure 4. Comparison of the length distribution of bottom-up assembled TMV-like particles (AFM topography image a_1 and histogram a_2) with particles preassembled in solution (AFM topography image b_1 and histogram b_2). In both cases, the VLPs were deposited on structured Si wafers. The box plot (top middle) shows the different length distributions obtained by the distinct assembly strategies, with median values (black dot), 50% particle populations between second/third quartiles (gray boxes), and lowest/largest values (lines) indicated. The expected maximum particle length of 135 nm, corresponding to the RNA template used, is labeled by the dotted line in the plot. For particle length determination, AFM tip convolution was taken into account.

RNAs' ends linked to the solid substrate at predetermined sites of a solid−liquid interface.

The polymer-patterned substrates allowed a complete control of spatial selectivity down to areas in the 100 nm range: TMV-like nanosticks were observed exclusively in the nonpassivated "holes" (see Figure 2a−f). Interestingly, a further improvement was achieved with samples where the PMMA mask was removed after chemical functionalization of the Si wafers. Here, subsequent self-assembly of TMV-like nanorods also occurred perfectly site-selectively, but with a much higher efficiency as in the experiments described above (Figure 3a,b). The molecular reasons underlying this amendment are not clear; however, these data prove that it is possible to grow arrays of TMV-based nanorods with increased densities.

The final lengths of the rods assembled on solid substrates were determined from AFM images processed to verify flat positioning of analyzed particles (Figure 4) by help of the software ImageJ. In all cases, tip convolution was taken into account. To allow for direct comparisons, VLPs grown in solution with the same RNA template (scaffolding 135 nm length upon complete encapsidation) were deposited on equally prepared substrates and measured in parallel. The average median apparent length of particles assembled bottom-up on surfaces was 96(±4) nm, with 17% between 115 and 135 nm, which significantly differed from 110(±4) nm determined for rods constituted in solution (P_{error} <0.0001 delimited by Mann−Whitney rank sum test), with 32% between 115 and 135 nm, respectively. These deviating length distributions are detailed for one experiment in Figure 4. Here it should be mentioned that the apparent lengths of preassembled TMVs in the same batch were different, depending on the method of characterization. With AFM, a slightly decreased average median apparent length of particles was determined, compared to the transmission electron microscopy (TEM) method (see Supporting Information Figure S3). This observation can be explained by differences in the interaction between VLPs and the corresponding substrate materials that were used for sample preparation and analysis and is in accordance with literature, where the influence of different substrate materials on the longitudinal dimensions of TMV particles was investigated.[43,44]

To find out whether RNase contaminations of the wafers, or nucleic acid attached enzyme molecules degrading or shielding portions of the RNA strands contributed to the discrepancy in the length between VLPs assembled bottom-up and those grown in solution (see Figure 4), intermediate products formed in the course of a bottom-up assembly experiment were analyzed for integrity and functionality of the RNA scaffolds (Figure 5). After both enzymatic treatments, that is, with Antarctic Phosphatase *in vitro*, and subsequently with T4 RNA ligase 1 *in situ* on linker-equipped wafers (as specified in the Experimental Methods section), excess RNA-containing solution was collected and subjected to electrophoretic analysis before and

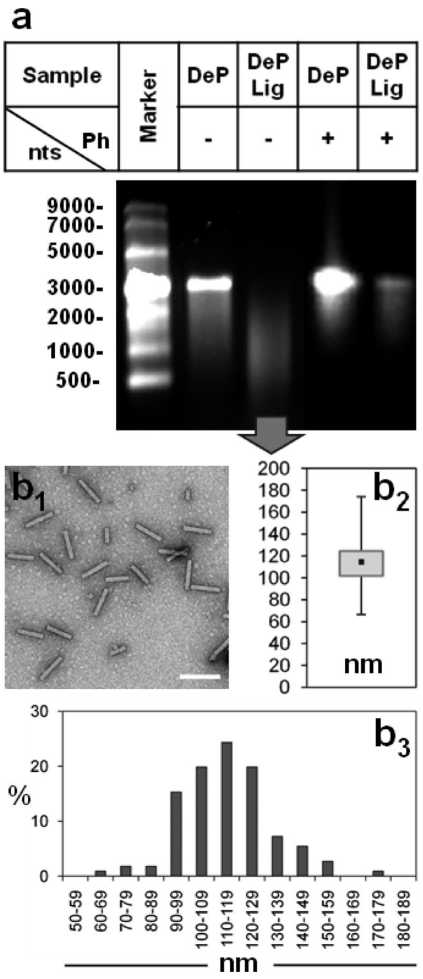

Figure 5. Influence of Antarctic Phosphatase, T4 RNA ligase 1 treatment and incubation on wafers on the capability of scaffold RNA to direct the assembly of TMV-like particles with CP. (a) RNA gel electrophoresis after enzymatic treatments (dephosphorylation, DeP; ligation, Lig) without and with subsequent phenol-based purification (Ph −/+); (b) particles after *in vitro* assembly with RNA treated with both enzymes but not phenol (corresponding to sample labeled with arrow). (b_1) Transmission electron micrograph after negative staining, bar: 200 nm; (b_2,b_3) box plot and histogram of length distribution for $n = 111$ particles, as determined by AFM on wafer substrates. The apparent median particle length was 114 nm (for details, see Figure 4, Experimental Methods, and Supporting Information Figure S3). Nucleotides (nts) of RNA marker bands.

after phenol extraction of proteins adsorbed to the nucleic acid template. Whereas the combination of both phosphatase and ligase strongly affected RNA mobility in the gel system applied, intact RNA was recovered to high amounts from this sample by protein removal (Figure 5a). A portion of the sample was incubated with assembly competent protein *in vitro* directly after its collection from the wafer and no further purification. TEM of negatively stained products and their length analysis revealed that rods were grown indistinguishable from those assembled with fresh RNA in solution (Figure 5b). These tests indicated that residual RNase contaminations as well as enzyme-caused hindrance of complete RNA encapsidation could be ruled out; hence interactions of the nascent rods with the surface might explain their decreased final average length in comparison to that of particles assembled freely floating.

Further evidence for this assumption comes from controls which shed additional light on individual stages of the *in situ* assembly procedure. In parallel tests, aliquots of assembly competent TMV CP were incubated on aldehyde-functionalized homogeneous Si wafers equipped with ssDNA linkers and treated with RNA scaffolds, as well, but without addition of RNA ligase. After the washing steps were applied, as described below, no TMV-like rods were found on the respective substrates, but lumps and fibers (Supporting Information Figure S2d), similar to the structures obtained in the absence of DNA linkers (Figure S2c). They probably represent surface-attached CP and nucleic acid aggregates not amenable for reorganization into VLPs, which also occurred as background structures on substrates supporting RNA-guided nanorod growth (Figure S2a,b). This is indicative of attractive interactions between substrates and protein and RNA building blocks, even after $NaBH_4$-mediated reduction of surface aldehydes into alcohols. Incubation of preformed virus-like rods on patterned Si wafers after removal of the PMMA mask and DNA linker immobilization resulted in an almost homogeneous coverage of these substrates, on both the areas functionalized with amine-coupled linkers and the amino-silanized areas initially protected by the polymer mask (Figure 3c,d). This finding evidenced that also the reconstituted helical viral protein coat can adsorb to the functionalized surfaces applied in this study, which may not only impede complete encapsidation of surface-bound RNA scaffolds but also compromise free accessibility of the bottom-up assembled architectures in intended subsequent applications.

Taken together, these tests also revealed that the stepwise construction approach combining a series of covalent linking and intermittent washing steps to build up RNA scaffolds only on predetermined patches is essential to achieve spatial selectivity of protein rod growth. End-immobilized, but otherwise floating, RNA strands harboring the TMV OAs then obviously compete for assembly competent CP with nonspecific substrate adhesion, with the cooperative nanotube growth being favored especially in the case of patterned substrates. The improved protein multimerization efficiency on these surfaces, containing remainders of the PMMA masks (to which TMV did not adhere significantly; data not shown) on silanized areas, might involve excluded volume effects mediated by polymer molecules at the solid−liquid interface. Such crowding is known to affect the free energy landscape of protein conformations, accelerating, for example, actin fiber and microtubule formation under suitable conditions.[45]

On the other hand, surface coverage with TMV-like particles in no case reached saturation, irrespective of whether grown *in situ*, or deposited in assembled state (in amounts sufficient to form 16 closed layers) from the same buffer as a control. Putative molecular reasons encompass limited availability of DNA linker or RNA strands, respectively, as well as physical constraints during the *in situ* assembly process. DNA linker binding efficiency was comparable between commercially produced aldehyde-terminated glass slides and glass substrates functionalized in parallel to the Si wafers in this study (data not shown), but significantly superior on the latter (Figure S1). This indicates that a limiting coverage with linkers can be largely excluded because their average density on routinely applied array substrates is 10^{12} oligonucleotides/cm^2,[46,47] which corresponds to a mean intermolecular distance of 10 nm. By contrast, no safe assumption is possible for the yield of T4 RNA ligase-accomplished ligation of long RNA to the DNA: since even under optimum conditions of quasi-monomolecular reactions only 30−50% efficiency are achieved,[48] 4500-fold excess of enzyme was used, though without subsequent quantification of reaction products.

The incomplete coverage of wafers even after treatment with preformed TMV-like nanotubes, however, yielded strong evidence for a major contribution of physical limitations on TMV CP enrichment at target sites. Helically assembled as well as mono- or oligomeric protein subunits exhibit a negative net charge under conditions of multimerization[49,50] and therefore are subject to repulsive electrostatic interactions with surfaces equipped with nucleic acids as well as with adjacent coat protein aggregates. Suci *et al.*[51] have investigated comparable inter-relationships between differently charged Si and polymer substrates, and Cowpea chlorotic mottle virus (CCMV) icosahedral particles with a pI of 3.8 similar to that of TMV. Their experiments have underscored the pivotal influence of electrostatic interactions on the resulting spatial distribution of viruses, the kinetic adsorption behavior of which could be described well by use of the Langmuir model with limitations found for conditions close to equilibrium.[51]

TMV particle densities obtained in other studies on different surfaces are mostly in agreement with this suggestion: hybridization of partially disassembled virus rods *via* an exposed 5′ portion of their RNA to oligodesoxynucleotides on solid substrates resulted in arrays quite comparable to those observed on patterned wafers (after PMMA removal) in our study,[28,32] whereas high-density deposition of TMV or M13 phage arrays was achieved by different technologies: planar self-organization into closed films occurred upon diffusion through polyelectrolyte multilayers;[26,31] densely packed arrays with rod orientation predominantly normal to the surface were generated by metal-to-thiol-linkage of the viral protein coat,[8,25] a method also applied, for example, to the icosahedral Cowpea mosaic virus CPMV;[30] and by photolithographic lift-off technology.[29] Close to complete coverage with random rod orientation was also possible by microcontact printing[27] and, interestingly, by hybridization of partially "stripped" TMV with their RNA ends to ssDNA probes on chitosan-modified surfaces.[34]

In conclusion, it is demonstrated for the first time that on wafers which are site-selectively functionalized with RNA the bottom-up assembly of TMV-like particles is possible. However, the surfaces and strategies combined in this study to achieve spatially selective wafer functionalization with RNA scaffolds governing the growth of TMV-like rods suffered from oppositional restrictions: Whereas nonspecific adhesive interactions were observed between linker-exposing patches and fully assembled virus-like rods, which may confine their subsequent accessibility, repulsive electrostatic forces are likely to limit the maximum coverage of the solid supports. This may be further affected by the efficiency of T4 RNA ligase upon intermolecular joining of long RNA strands with immobilized DNA and by steric hindrance due to the degrees of spatial freedom needed for realizing the bidirectional TMV assembly process using different types of protein aggregates on surface-attached RNA.

Although the whole process will therefore need further optimization, our findings demonstrate that micropatterned, nucleic acid equipped technical substrates offer a so far unique opportunity for an inducible, kinetically controlled, and site-selective bottom-up growth of true nanostructures, thus bridging the nano- and the microworld.

The DNA-mediated linkage of the assemblies to sites of interest prove to withstand extended washing of the freshly grown nanorods with 60 mL/min flow, corresponding to 2.4 cm/s buffer stream inverting direction three times per second, in all experiments. This harsh treatment exceeded flow rates routinely applied in many lab-on-a-chip microfluidic devices.[52−54] Dried arrays even remained unaffected by flowing water of 25 mL/s for 2 min or streaming 0.1% SDS for 30 s, being removed from the wafers only after two min ultrasound exposure at 40 kHz (data not shown), which completed test series on the robustness of the ensembles. Various engineered and natural variants of TMV CP are suitable for self-assembly,[17,22,23,25,41,49,55] leading to nanotubes exposing distinctive reactive groups, which may be addressed with high specificity. This allows coupling of multiple bioactive or sensor functions to the polyvalent viral backbone,[10] which gains high stability against enzymes and chemical or physical damage after the RNA has been completely packaged.[56] So far, as detailed above, predominantly suspended or surface-deposited fully assembled virus particles

have been exploited as biotemplates to create metallic or catalytically active nanorods.[16,20,21,33,57,58] A combination of those functionalization technologies with the array production strategy based on monomeric building blocks, as established in this study, might lead to novel integration procedures of applicable hybrid nanorod arrays[2] into predefined, but difficult to access sites of advanced microdevices.

EXPERIMENTAL METHODS

Aldehyde Functionalization of Si Wafers and Control Glass Slides. Si wafers (100, Wacker, Germany) were heated in an oven for 1 h at 1100 °C and cut into suitable pieces. These were treated with a dry ice stream (snow-jet) directly after cutting, boiled in ethanol for 15 min, dried intermittently, boiled in an aqueous solution consisting of 1 part of 25 wt % NH_3 (aq), 1 part of 30 wt % H_2O_2 (aq), and 5 parts of H_2O for 10 min, washed with H_2O, boiled 10 min in an aqueous solution consisting of 1 part 32 wt % HCl (aq), 30 wt % H_2O_2 (aq), and 5 parts of H_2O, and washed with H_2O again. The surfaces were dried in a stream of nitrogen and used for functionalization immediately.

Amino silanization of the cleaned or prestructured (see below) Si wafers was done by gas phase silanization with aminopropyltriethoxysilane under nitrogen atmosphere. Si wafer pieces were placed over a beaker containing pure aminopropyltriethoxysilane at room temperature (RT) in dry nitrogen for 40 min. Afterward, the silanized samples were incubated in a 1% glutardialdehyde solution in ambient atmosphere for 30 min, washed with H_2O, and dried in a stream of nitrogen (procedure modified from Feng *et al.*[35]). For optimization of DNA linker and RNA binding, glass slides were prepared by using the same protocol.

In order to prestructure Si wafers, they were coated with a polymer blend after cleaning,[37,40,59] which consisted of a molar 1:1 mixture of polystyrene (PS) and polymethylmethacrylate (PMMA) in methyl−ethyl−ketone with a total polymer concentration of 2 mg/mL. Twenty microliters of this solution was coated with a spin coater at 50 rps for 30 s onto the Si wafers. The resulting polymer pattern was treated with cyclohexane in an ultrasonic bath for 10 min to selectively remove the PS from the surface, which uncovers the Si wafer in these areas. Si wafers structured that way were then amino-silanized and aldehyde-functionalized as described above.

An alternative strategy toward patterned substrates selectively functionalized with aldehyde, but devoid of a polymer mask upon nucleic acid equipment and nanotube assembly, started with homogeneous gas phase amino silanization of cleaned Si wafer pieces as above. The silanized surfaces were then patterned by coating a 1:1 (PS/PMMA) polymer blend onto the aminopropyltriethoxysilane film (experimental conditions as before). Treatment with cyclohexane for 10 min in an ultrasonic bath developed the desired PMMA masks. The Si wafer pieces structured in such a manner were then immersed in a 1% glutardialdehyde solution in water for 30 min, followed by a treatment with glacial acetic acid in an ultrasonic bath to finally remove the PMMA mask. The resulting locally aldehyde-exposing Si wafers lacking a permanent polymer pattern were used for ssDNA linker coupling, ligation of RNA scaffolds, and bottom-up self-assembly experiments, the results of which are shown in Figure 3.

DNA Linker Immobilization on Functionalized Si Wafers: Optimization Procedure. Immobilization of DNA linker molecules was optimized on aldehyde-functionalized wafers. Initial experiments included glass slides prepared *via* the same procedure and commercially available aldehydesilane-coated slides (Nexterion Slide AL, Schott, Jena, Germany). 5′-Terminally amino-modified single-stranded DNA (ssDNA) linker molecules (purchased from Metabion; Martinsried, Germany) with the following nucleotide sequences were utilized: *5′-NH_2-GCACCACGTGTGATTACGGACA-CAATCCG-3* (TestLinker(+)_NH_2) and *5′-NH_2-TGGGCCCCTACCG-GGGGTAACGGGGGG-3* (TestLinker(−)_NH_2).

The linker molecules were diluted in 3× SSC (sodium salt citrate buffer from a 20× SSC stock solution[60]) to the desired concentration (0.01−10 pmol/μL) and applied to the functionalized surfaces in a final volume of 3−5 μL. After incubation in a humid chamber for 15−30 min and a series of washing steps (2 × 2 min 0.2% SDS, 2 × 2 min ddH_2O, 1 × 1 min ddH_2O), the substrates were incubated in a solution of 0.25% $NaBH_4$ in [PBS[60] buffer/ethanol (3:1)] under slight shaking in order to react superfluous aldehyde groups to nonreactive alcohol functions and convert Schiff bases into stable amines. For the evaluation of linker binding efficiencies, ssDNA probe molecules (Metabion) complementary in their nucleotide sequence to TestLinker(+)_NH_2 and with a 5′-terminal biotin hapten (*5′-biotin-CGGATTGTGTCCGTAATCACACGTGGTGC-3′*) were hybridized to the immobilized linkers. Hybridization was carried out for 16−18 h at 37 °C with 5−6 ng/mL probe in 3× SSC buffer. After several washing steps (2 × 2 min 0.2% SDS, 2 × 2 min ddH_2O, 1 × 1 min ddH_2O), specifically hybridized biotinylated probes were detected by a chemiluminescence reaction. To this aim, the substrates were washed with DIG washing buffer for 5 min (DIG buffers according to the DIG Application Manual for Filter Hybridization; Roche Cat #11438425001; except that DIG buffer 3 was prepared without $MgCl_2$) and blocked for 30−40 min in DIG blocking solution. A 1/10 000 dilution of streptavidin−alkaline phosphatase (streptavidin−AP) conjugate (Roche; Cat #11093266910) in DIG blocking buffer was applied and incubated for 30 min under gentle shaking. Afterward, substrates were washed for 2 × 10 min with DIG washing buffer and rinsed for 1 min with DIG buffer 3. For detection of the biotin−streptavidin coupling, a chemoluminescence-generating substrate of alkaline phosphatase (CDP-Star; ROCHE; Cat #12041677001) was diluted 1/500 in DIG buffer 3 and applied to the surfaces. Substrates were then sealed into transparent plastic bags, placed in an exposition cassette, and incubated for 15 min at 37 °C prior to the exposition of an X-ray film (SuperRX, Fujifilm) for 3−4 h.

RNA Ligation and Induced Assembly of TMV-like Nanotubes on Unstructured and Patterned Surfaces. Under the conditions described above, both homogeneously functionalized and patterned DNA-linker-exposing surfaces were prepared and equipped with genetically engineered RNA strands. The amino-functionalized ssDNA linker molecule "RNA_anchor" (*5′-phosphate-TTAAAAAAAAAAAAAAAAAA-3′NH_2*) was synthesized by Metabion (Martinsried, Germany); RNA *in vitro* transcripts (2884 nts in length) containing the TMV OAs were prepared as described.[41] The RNA transcripts were enzymatically ligated to one end of the linkers as follows: a mixture containing 2−5 ng/μL dephosphorylated RNA, 1 U/μL RNase inhibitor mix (NEB), and 1 U/μL T4 RNA ligase 1 (NEB) was prepared in 1× T4 RNA ligase buffer (corresponding to ∼4500-fold enzyme excess). Prior to the addition of enzyme and inhibitor mix, the solution was heated to 95 °C for 3 min and cooled on ice. Depending on the substrate size, 50−100 μL of complete ligation mixture was applied and incubated in a humid chamber at 37 °C for 3 h. After ligation, preparations were washed in 2× SSC/0.2% SDS (2 × 10 min), 2× SSC (1 × 10 min), 0.2 SSC (1 × 10 min) and ddH_2O (2 × 5 min) under vigorous shaking at RT.

Specimens were then supplemented with assembly competent TMV coat protein preparations under conditions inducing and promoting growth of TMV-like nanotubes *in situ*,[41] as optimized for the two-phase system. Before starting assembly reactions, RNA-exposing silica wafers were rinsed with 50 mM SPP (sodium potassium phosphate buffer, pH 7.2) for 5−10 min. The bottoms of sterile plastic Petri dishes were covered with Parafilm, onto which Parafilm posts (about 1 mm height) were adhered to serve as support for the wafers; 50−200 μL of TMV CP (1.3 μg/μL in 50 mM SPP), depending on the wafer size, was applied between the spacers and the respective substrate placed on top, with its RNA-equipped surface pointing toward

the bottom. This arrangement was incubated overnight in a humid chamber at 30 °C. The substrates were washed under shaking for 2 × 10 min in 0.2% SDS and 2 × 10 min in ddH_2O before they were dried in a nitrogen stream and analyzed by atomic force microscopy (AFM).

Analysis by AFM. Images were taken with a Multimode AFM connected to a Nanoscope IIIa controller (Digital Instruments, USA) and show raw data. The AFM was operated in air at ambient temperature in intermittent contact mode. NSC 36 silicon cantilevers (MicroMash, USA) were used with typical force constants between 0.6 and 1.8 N/m. Figure S2 shows successful self-assembly events on a homogeneously functionalized Si wafer and control reactions lacking DNA linkers or ligase. For statistical investigation of the particle length distribution, the AFM images were modified in that way that only those particles were evaluated which were lying parallel to the substrate. Length determination was carried out with the software ImageJ, v1.43.[61] Tip convolution was taken into account in all cases by using a geometrical model to calculate the error. For this purpose, the tip-specific geometrical properties (tip angle 40°, tip radius 9 nm) were used, while the TMV particles were assumed as structures with rectangular cross section. To calculate the effect of tip convolution, we used allophone particles (natural spherical nanoparticles with narrow size distribution between 5 and 6 nm in diameter). These diameters of the particles were determined to 6 nm by SEM and to 12 nm by AFM for the AFM tip type used in this work. Tip deconvolution was carried out by the software Scanning Probe Image Processor (SPIP, version 4.2.6.0, Image Metrology, Denmark).

Analysis of Intermediate RNA States in the Course of Bottom-Up Assembly. After enzymatic treatment with Antarctic Phosphatase *in vitro* and again after subsequent incubation with T4 RNA ligase 1 *in situ* on linker-equipped wafers (see above), excess RNA-containing solution was collected and divided into aliquots, which were subjected to different procedures and analyzed in agarose gels or used as scaffolds for *in vitro* encapsidation of scaffold RNA in solution. Prior to electrophoresis, one of each portions was treated only with denaturating RNA sample buffers,[62] whereas a second portion was treated with phenol/chloroform to extract proteins adsorbed to the RNA.[60] The samples were diluted to a volume of 200 μL and, after phenol extraction, concentrated to the original volume using *n*-butanol.[60] Then, 50−500 ng of RNA was applied for sample preparation, separated on 1% agarose gels in 1× TBE buffer for 2 h at 5 V/cm, and stained with ethidium bromide. An aliquot of the RNA ligation mixture incubated with both enzymes was combined with assembly competent protein directly after its collection from the wafer and analyzed by transmission electron microscopy after negative staining with UAc,[41] as well as on wafers by AFM (as described above) to determine the length distribution of assembly products.

Acknowledgment. We are grateful to S. Kober for the preparation of several batches of TMV, and our gardeners A. Allinger and D. Gotthardt for taking great care of the plants. We thank the Baden-Wuerttemberg-Stiftung, Network of Competence "Functional Nanostructures", for funding the project, and the DFG SPP1165 and the CFN for subsidiary financial support.

Supporting Information Available: Three supplementary figures, showing results of optimization and control experiments. Figure S1: DNA linker immobilization on functionalized Si wafers. Figure S2: Assembly of TMV-like nanotubes on homogeneously functionalized unstructured substrates (including control samples). Figure S3: Apparent length distributions of TMV-like particles; comparison of length measurements by TEM and AFM methodology. This material is available free of charge *via* the Internet at http://pubs.acs.org.

REFERENCES AND NOTES

1. Alivisatos, P. The Use of Nanocrystals in Biological Detection. *Nat. Biotechnol.* **2004**, *22*, 47–52.
2. Mann, S. Self-Assembly and Transformation of Hybrid Nano-objects and Nanostructures under Equilibrium and Non-equilibrium Conditions. *Nat. Mater.* **2009**, *8*, 781–792.
3. Wang, L.; Montagne, F.; Hoffmann, P.; Heinzelmann, H.; Pugin, R. Hierarchical Positioning of Gold Nanoparticles into Periodic Arrays Using Block Copolymer Nanoring Templates. *J. Colloid Interface Sci.* **2011**, *356*, 496–504.
4. Erickson, D.; Mandal, S.; Yang, A. H.; Cordovez, B. Nanobiosensors: Optofluidic, Electrical and Mechanical Approaches to Biomolecular Detection at the Nanoscale. *Microfluid. Nanofluid.* **2008**, *4*, 33–52.
5. Lewandowski, D. Genus Tobamovirus. In *Virus Taxonomy. 8th Report of the International Committee on Taxonomy of Viruses*; Fauquet, C. M., Mayo, M. A., Maniloff, J., Desselberger, U., Ball, L. A., Eds.; Elsevier/Academic Press: London, 2005; pp 1009−1014.
6. Li, K.; Nguyen, H. G.; Lu, X.; Wang, Q. Viruses and Their Potential in Bioimaging and Biosensing Applications. *Analyst* **2010**, *135*, 21–27.
7. Young, M.; Willits, D.; Uchida, M.; Douglas, T. Plant Viruses as Biotemplates for Materials and Their Use in Nanotechnology. *Annu. Rev. Phytopathol.* **2008**, *46*, 361–384.
8. Gerasopoulos, K.; McCarthy, M.; Banerjee, P.; Fan, X.; Culver, J. N.; Ghodssi, R. Biofabrication Methods for the Patterned Assembly and Synthesis of Viral Nanotemplates. *Nanotechnology* **2010**, *21*, 055304–055311.
9. Soto, C. M.; Ratna, B. R. Virus Hybrids as Nanomaterials for Biotechnology. *Curr. Opin. Biotechnol.* **2010**, *21*, 426–438.
10. Mao, C.; Liu, A.; Cao, B. Virus-Based Chemical and Biological Sensing. *Angew. Chem., Int. Ed.* **2009**, *48*, 6790–6810.
11. Wu, Z.; Mueller, A.; Degenhard, S.; Ruff, S. E.; Geiger, F.; Bittner, A.; Wege, C.; Krill, C., III. Enhancing the Magnetoviscosity of Ferrofluids by the Addition of Biological Nanotubes. *ACS Nano* **2010**, *4*, 4531–4538.
12. Wu, Z.; Zierold, R.; Mueller, A.; Ruff, S. E.; Ma, C.; Khan, A. A.; Geiger, F.; Sommer, B. A.; Knez, M.; Nielsch, K.; Bittner, A. M.; Wege, C.; Krill, C., III. Preparation and Magnetoviscosity of Nanotube Ferrofluids by Viral Scaffolding and ALD on Porous Templates. *Phys. Status Solidi B* **2010**, *247*, 2412–2423.
13. Butler, P. J. Self-Assembly of Tobacco Mosaic Virus: The Role of an Intermediate Aggregate in Generating Both Specificity and Speed. *Philos. Trans. R. Soc. London, Ser. B* **1999**, *354*, 537–550.
14. Lauffer, M. A. *Entropy-Driven Processes in Biology*; Springer-Verlag: Heidelberg, 1975; Vol. 20.
15. Balci, S.; Noda, K.; Bittner, A. M.; Kadri, A.; Wege, C.; Jeske, H.; Kern, K. Self-Assembly of Metal-Virus Nanodumbbells. *Angew. Chem., Int. Ed.* **2007**, *46*, 3149–3151.
16. Knez, M.; Sumser, M.; Bittner, A. M.; Wege, C.; Jeske, H.; Martin, T. P.; Kern, K. Spatially Selective Nucleation of Metal Clusters on the Tobacco Mosaic Virus. *Adv. Funct. Mater.* **2004**, *14*, 116–124.
17. Lim, J.-S.; Kim, S.-M.; Lee, S.-Y.; Stach, E. A.; Culver, J. N.; Harris, M. T. Quantitative Study of Au(III) and Pd(II) Ion Biosorption on Genetically Engineered Tobacco Mosaic Virus. *J. Colloid Interface Sci.* **2010**, *342*, 455–461.
18. Smith, M. L.; Lindbo, J. A.; Dillard-Telm, S.; Brosio, P. M.; Lasnik, A. B.; McCormick, A. A.; Nguyen, L. V.; Palmer, K. E. Modified Tobacco Mosaic Virus Particles as Scaffolds for Display of Protein Antigens for Vaccine Applications. *Virology* **2006**, *348*, 475–488.
19. Dedeo, M. T.; Duderstadt, K. E.; Berger, J. M.; Francis, M. B. Nanoscale Protein Assemblies from a Circular Permutant of the Tobacco Mosaic Virus. *Nano Lett.* **2010**, *10*, 181–186.
20. Górzny, M.; Walton, A. S.; Evans, S. D. Synthesis of High-Surface-Area Platinum Nanotubes Using a Viral Template. *Adv. Funct. Mater.* **2010**, *20*, 1295–1300.
21. Kobayashi, M.; Seki, M.; Tabata, H.; Watanabe, Y.; Yamashita, I. Fabrication of Aligned Magnetic Nanoparticles Using Tobamoviruses. *Nano Lett.* **2010**, *10*, 773–776.
22. Frolova, O. Y.; Petrunia, I. V.; Komarova, T. V.; Kosorukov, V. S.; Sheval, E. V.; Gleba, Y. Y.; Dorokhov, Y. L. Trastuzumab-Binding Peptide Display by Tobacco Mosaic Virus. *Virology* **2010**, *407*, 7–13.
23. Kadri, A.; Maiss, E.; Amsharov, N.; Bittner, A. M.; Balci, S.; Kern, K.; Jeske, H.; Wege, C. Engineered Tobacco Mosaic Virus Mutants with Distinct Physical Characteristics in

Planta and Enhanced Metallization Properties. *Virus Res.* **2011**, *157*, 35–46.
24. Knez, M.; Sumser, M. P.; Bittner, A. M.; Wege, C.; Jeske, H.; Hoffmann, D. M.; Kuhnke, K.; Kern, K. Binding the Tobacco Mosaic Virus to Inorganic Surfaces. *Langmuir* **2004**, *20*, 441–447.
25. Royston, E.; Ghosh, A.; Kofinas, P.; Harris, M. T.; Culver, J. N. Self-Assembly of Virus-Structured High Surface Area Nanomaterials and Their Application as Battery Electrodes. *Langmuir* **2008**, *24*, 906–912.
26. Steinmetz, N. F.; Bock, E.; Richter, R. P.; Spatz, J. P.; Lomonossoff, G. P.; Evans, D. J. Assembly of Multilayer Arrays of Viral Nanoparticles *via* Biospecific Recognition: A Quartz Crystal Microbalance with Dissipation Monitoring Study. *Biomacromolecules* **2008**, *9*, 456–462.
27. Balci, S.; Leinberger, D. M.; Knez, M.; Bittner, A. M.; Boes, F.; Kadri, A.; Wege, C.; Jeske, H.; Kern, K. Printing and Aligning Mesoscale Patterns of Tobacco Mosaic Viruses on Surfaces. *Adv. Mater.* **2008**, *20*, 2195–2200.
28. Yi, H.; Rubloff, G. W.; Culver, J. N. TMV Microarrays: Hybridization-Based Assembly of DNA-Programmed Viral Nanotemplates. *Langmuir* **2007**, *23*, 2663–2667.
29. Chen, X.; Gerasopoulos, K.; Guo, J.; Brown, A.; Wang, C.; Ghodssi, R.; Culver, J. N. Virus-Enabled Silicon Anode for Lithium-Ion Batteries. *ACS Nano* **2010**, *4*, 5366–5372.
30. Cheung, C. L.; Camarero, J. A.; Woods, B. W.; Lin, T.; Johnson, J. E.; De Yoreo, J. J. Fabrication of Assembled Virus Nanostructures on Templates of Chemoselective Linkers Formed by Scanning Probe Nanolithography. *J. Am. Chem. Soc.* **2003**, *125*, 6848–6849.
31. Yoo, P. J.; Nam, K. T.; Qi, J.; Lee, S. K.; Park, J.; Belcher, A. M.; Hammond, P. T. Spontaneous Assembly of Viruses on Multilayered Polymer Surfaces. *Nat. Mater.* **2006**, *5*, 234–240.
32. Tan, W. S.; Lewis, C. L.; Horelik, N. E.; Pregibon, D. C.; Doyle, P. S.; Yi, H. Hierarchical Assembly of Viral Nanotemplates with Encoded Microparticles *via* Nucleic Acid Hybridization. *Langmuir* **2008**, *24*, 12483–12488.
33. Chen, X.; Gerasopoulos, K.; Guo, J.; Brown, A.; Ghodssi, R.; Culver, J. N.; Wang, C. High Rate Performance of Virus Enabled 3d N-Type Si Anodes for Lithium-Ion Batteries. *Electrochim. Acta* 2011, DOI: 10.1016/j.electacta.2011.03.037.
34. Yi, H.; Nisar, S.; Lee, S. Y.; Powers, M. A.; Bentley, W. E.; Payne, G. F.; Ghodssi, R.; Rubloff, G. W.; Harris, M. T.; Culver, J. N. Patterned Assembly of Genetically Modified Viral Nanotemplates *via* Nucleic Acid Hybridization. *Nano Lett.* **2005**, *5*, 1931–1936.
35. Feng, J.; Gao, C.; Wang, B.; Shen, J. Co-patterning Chitosan and Bovine Serum Albumin on an Aldehyde-Enriched Glass Substrate by Microcontact Printing. *Thin Solid Films* **2004**, *460*, 286–290.
36. Berlinger, A.; Gliemann, H.; Barczewski, M.; Durigon, P. E. R.; Siqueira Petri, D. F.; Schimmel, T. Influence of Sulphonation on Polymer and Polymer Blend Surfaces Studied by Atomic Force Microscopy. *Surf. Interface Anal.* **2001**, *32*, 144–147.
37. Gliemann, H.; Almeida, A. T.; Freitas, D.; Petri, S.; Schimmel, T. Nanostructure Formation in Polymer Thin Films Influenced by Humidity. *Surf. Interface Anal.* **2007**, *39*, 1–8.
38. Tanaka, K.; Takahara, A.; Kajiyama, T. Film Thickness Dependence of the Surface Structure of Immiscible Polystyrene/Poly(methyl methacrylate) Blends. *Macromolecules* **1996**, *29*, 3232–3239.
39. Cui, L.; Ding, Y.; Li, X.; Wang, Z.; Han, Y. Solvent and Polymer Concentration Effects on the Suface Morphology Evolution of Immiscible Polystyrene/Poly(methylmethacrylate) Blends. *Thin Solid Films* **2004**, *515*, 2038–3048.
40. Walheim, S.; Boltau, M.; Mlynek, J.; Krausch, G.; Steiner, U. Structure Formation *via* Polymer Demixing in Spin-Cast Films. *Macromolecules* **1997**, *30*, 4995–5003.
41. Mueller, A.; Kadri, A.; Jeske, H.; Wege, C. *In Vitro* Assembly of Tobacco Mosaic Virus Coat Protein Variants Derived from Fission Yeast Expression Clones or Plants. *J. Virol. Methods* **2010**, *166*, 77–85.
42. Wittmann, C.; del Campo, A.; Bruce, I. J. Immobilisation of DNA on Chips I. In *Topics in Current Chemistry*; Wittmann, C., Ed.; Springer: Berlin, 2005; Vol. 260.
43. Britt, D. W.; Buijs, J.; Hlady, V. Tobacco Mosaic Virus Adsorption on Self-Assembled and Langmuir–Blodgett Monolayers Studied by TIRF and SFM. *Thin Solid Films* **1998**, *327–329*, 824–828.
44. Dubrovin, E.; Kirikova, M.; Novikov, V.; Drygin, Y.; Yaminsky, I. Study of the Peculiarities of Adhesion of Tobacco Mosaic Virus by Atomic Force Microscopy. *Colloid J.* **2004**, *66*, 673–678.
45. Minton, A. P. Implications of Macromolecular Crowding for Protein Assembly. *Curr. Opin. Struct. Biol.* **2000**, *10*, 34–39.
46. Pirrung, M. C. How to Make a DNA Chip. *Angew. Chem., Int. Ed.* **2002**, *41*, 1276–1289.
47. Zammatteo, N.; Jeanmart, L.; Hamels, S.; Courtois, S.; Louette, P.; Hevesi, L.; Remacle, J. Comparison between Different Strategies of Covalent Attachment of DNA to Glass Surfaces To Build DNA Microarrays. *Anal. Biochem.* **2000**, *280*, 143–150.
48. Persson, T.; Willkomm, D. K.; Hartmann, R. K. T4 RNA Ligase. In *Handbook of RNA Chemistry*; Hartmann, R. K., Bindereif, A., Schön, A., Westhof, E., Eds.; Wiley-VCH Verlag GmbH: Weinheim, Germany, 2008; pp 53–74.
49. Bendahmane, M.; Koo, M.; Karrer, E.; Beachy, R. N. Display of Epitopes on the Surface of Tobacco Mosaic Virus: Impact of Charge and Isoelectric Point of the Epitope on Virus–Host Interactions. *J. Mol. Biol.* **1999**, *290*, 9–20.
50. Zaitlin, M. Tobacco Mosaic Virus. *AAB Descr. Plant Viruses* **2000**, *370*, 1–13.
51. Suci, P. A.; Klem, M. T.; Douglas, T.; Young, M. Influence of Electrostatic Interactions on the Surface Adsorption of a Viral Protein Cage. *Langmuir* **2005**, *21*, 8686–8693.
52. Chen, I. J.; Eckstein, E. C.; Lindner, E. Computation of Transient Flow Rates in Passive Pumping Micro-Fluidic Systems. *Lab Chip* **2009**, *9*, 107–114.
53. Gossett, D. R.; Weaver, W. M.; Mach, A. J.; Hur, S. C.; Tse, H. T.; Lee, W.; Amini, H.; Di Carlo, D. Label-Free Cell Separation and Sorting in Microfluidic Systems. *Anal. Bioanal. Chem.* **2010**, *397*, 3249–3267.
54. Liu, K.-K.; Wu, R.-G.; Chuang, Y.-J.; Khoo, H. S.; Huang, S.-H.; Tseng, F.-G. Microfluidic Systems for Biosensing. *Sensors* **2010**, *10*, 6623–6661.
55. McCormick, A. A.; Palmer, K. E. Genetically Engineered Tobacco Mosaic Virus as Nanoparticle Vaccines. *Expert Rev. Vaccines* **2008**, *7*, 33–41.
56. Klug, A. The Tobacco Mosaic Virus Particle: Structure and Assembly. *Philos. Trans. R. Soc. London, Ser. B* **1999**, *354*, 531–535.
57. Nam, Y. S.; Magyar, A. P.; Lee, D.; Kim, J. W.; Yun, D. S.; Park, H.; Pollom, T. S., Jr.; Weitz, D. A.; Belcher, A. M. Biologically Templated Photocatalytic Nanostructures for Sustained Light-Driven Water Oxidation. *Nat. Nanotechnol.* **2010**, *5*, 340–344.
58. Manocchi, A. K.; Horelik, N. E.; Lee, B.; Yi, H. Simple, Readily Controllable Palladium Nanoparticle Formation on Surface-Assembled Viral Nanotemplates. *Langmuir* **2010**, *26*, 3670–3677.
59. Geldhauser, T.; Walheim, S.; Schimmel, T.; Leiderer, P.; Boneberg, J. Influence of the Relative Humidity on the Demixing of Polymer Blends on Prepatterned Substrates. *Macromolecules* **2009**, *43*, 1124–1128.
60. Sambrook, J.; Russell, D. W. *Molecular Cloning: A Laboratory Manual*, 3rd ed.; Cold Spring Harbor Laboratory Press: Cold Spring Harbor, NY, 2001.
61. Rasband, W. S. *ImageJ*; U.S. National Institutes of Health, Bethesda, MD, 1997–2011; http://imagej.nih.gov/ij/.
62. Liu, Y. C.; Chou, Y. C. Formaldehyde in Formaldehyde/Agarose Gel May Be Eliminated without Affecting the Electrophoretic Separation of RNA Molecules. *Biotechniques* **1990**, *9*, 558–560.